PCCP

PAPER

View Article Online
View Journal | View Issue

Cite this: *Phys. Chem. Chem. Phys.*, 2023, **25**, 14869

Non-invasive monitoring of the growth of metal–organic frameworks (MOFs) *via* Raman spectroscopy†‡

Magdalene W. S. Chong, *[a] Andrew J. Parrott, *[b] David J. Ashworth, [cd] Ashleigh J. Fletcher [c] and Alison Nordon [ab]

Received 3rd March 2023,
Accepted 5th May 2023

DOI: 10.1039/d3cp01004j

rsc.li/pccp

The applicability of Raman spectroscopy for phase discrimination of metal–organic frameworks (MOFs) has been demonstrated with F4_MIL-140A(Ce) and F4_UiO-66(Ce); analogues prepared from the same metal and ligand sources. Each analogue exhibits unique Raman peaks, with significant differences in the low frequency region, which is more sensitive to structural variations. Non-invasive Raman monitoring of F4_MIL-140A(Ce) synthesis indicated evolution of a unique MOF Raman peak with reaction progress; conversion of this Raman signal to extent of crystallisation was in good agreement with reported reaction kinetics determined *via* a synchrotron diffraction method. Additionally, Raman spectroscopy indicated initial rapid consumption of the nitric acid modulator present in the reaction coinciding with an expected high probability of nucleation. Raman spectroscopy is a promising technique for rapid screening of MOFs and can be used to study the mechanism of their formation *in situ* with kinetic insight into both the solution and solid phases of the reaction medium.

Introduction

Understanding of crystallisation is fundamental to many industrial processes[1] and has presented a challenge in the commercialisation of metal–organic frameworks (MOFs).[2] The ability to reliably scale-up MOF synthesis is required if these materials are to be routinely deployed for tackling global energy,[3,4] healthcare,[5] and environmental[6,7] challenges. Advances in *in situ* monitoring of MOF formation are still in their relative infancy and are predominantly *via* methods involving complex and expensive instrumentation that cannot be easily deployed in a typical research laboratory or industrial environment, such as relying on a synchrotron[8–10] or similarly specialised facilities.[11] There are few examples using methods more easily applied in a typical laboratory, such as infrared[12,13] and Raman[14–17] spectroscopy, which can be deployed at the process instead of transporting the process to the analytical technique. An advantage to using vibrational spectroscopy is that the behaviour of different species within the reaction medium can be investigated. Within a MOF reaction mixture, Raman spectroscopy has been used to distinguish between MOF product, prenucleation building units, and the ligand precursor in the solid and solute forms.[16] Infrared spectroscopy has been suggested as a suitable technique to study the role of the solution species of acid modulator and solvent in MOF formation.[12] These last two examples used invasive probes, which have demonstrated a propensity for fouling or encrustation,[18–21] therefore the impact of their presence upon nucleation and crystallisation cannot be disregarded.

Non-invasive techniques remove the need for direct contact with the analyte,[22] which can mitigate any potential undesired effects arising from an in-line measurement mode. Non-invasive Raman spectroscopy has been widely adopted in the pharmaceutical industry,[23,24] including applications in various processes after crystallisation.[25–28] An advantage offered by Raman spectroscopy is polymorph discrimination, with non-invasive Raman being used for polymorph detection and quantification during crystallisation[29] and quantification of isomers in the solid state.[30] In particular, non-invasive probes, that are fibre-coupled to

[a] *WestCHEM, Department of Pure and Applied Chemistry and EPSRC Future Continuous Manufacturing and Advanced Crystallisation Research Hub, University of Strathclyde, 99 George Street, Glasgow, G1 1RD, UK. E-mail: magdalene.chong@strath.ac.uk*
[b] *WestCHEM, Department of Pure and Applied Chemistry and Centre for Process Analytics and Control Technology (CPACT), University of Strathclyde, 295 Cathedral Street, Glasgow, G1 1XL, UK. E-mail: andrew.parrott@strath.ac.uk*
[c] *Department of Chemical and Process Engineering, University of Strathclyde, James Weir Building, 75 Montrose Street, Glasgow, G1 1XJ, UK*
[d] *Strathclyde Institute of Pharmacy & Biomedical Sciences (SIPBS), University of Strathclyde, 161 Cathedral Street, G4 0RE, Glasgow, UK*

† All data underpinning this publication are openly available from the University of Strathclyde KnowledgeBase at https://doi.org/10.15129/801889bb-e2bf-425f-85ae-54ee12aaa7ce.

‡ Electronic supplementary information (ESI) available. See DOI: **https://doi.org/10.1039/d3cp01004j**

process Raman instruments, have been employed with a variety of vessels ranging from jacketed reaction vessels[30] to nuclear magnetic resonance (NMR) tubes[31] and even microfluidics.[32] As crystallisation (and solvothermal MOF formation) is inherently a two-phase process, Raman spectroscopy offers a route to obtaining data simultaneously from both phases non-invasively. The applicability of non-invasive Raman spectroscopy to *in situ* monitoring of MOF formation has recently been demonstrated for microscopy of a reaction in a vial[33] and mechanochemical synthesis.[34]

Raman spectroscopy has proved an alternative technique to more time-consuming analytical methods for rapid screening of materials, with sensitivity demonstrated for low levels (2% by mass) of analyte.[35] In this area, the development of THz Raman (or low frequency Raman) spectroscopy has enabled access to unique bands in the low frequency region for polymorph discrimination, which has been exploited in the pharmaceutical industry where polymorph certainty is paramount.[36] Predicted properties in the THz Raman region[37,38] suggested its applicability to MOF research, with few reports thus far studying MOFs by THz Raman.[39] THz Raman has facilitated studies into libration modes in MOFs,[40,41] including responses to adsorbed gas molecules,[42] and the methyl-rotation dynamics in zeolitic imidazolate frameworks.[43] THz Raman has demonstrated sensitivity to the open and closed phases of flexible frameworks,[44–46] which suggests potential in discriminating between analogues prepared from the same metal and ligand sources. Most of the studies rely on microscopy, which only permits highly localised sampling and are not easily deployed for *in situ* monitoring of laboratory or industrial processes. A small sampling area comparable to the size of one crystal may mean all phase changes occurring in the bulk reaction are not captured.[33] Another disadvantage to localised sampling is the potential for heating of the area of irradiation, and thus non-representative sampling of the bulk reaction medium.[47]

Here, deployment of non-invasive Raman spectroscopy in two areas of MOF research is demonstrated (Fig. 1). There has been relatively recent interest in Ce(IV) MOFs[48,49] and two Ce systems F4_MIL-140A(Ce) and F4_UiO-66(Ce) may be prepared *via* mild synthetic conditions.[8] Analysis of the two Ce MOFs by Raman and THz Raman spectroscopy indicated unique peaks corresponding to each analogue evident by both techniques, with significant differences in the THz region (Fig. 1(a)). Both MOFs may be prepared *via* aqueous synthesis, with water offering the advantage of being a weak Raman scatterer.[50] Non-invasive Raman monitoring was successfully used to detect the formation of both MOFs (Fig. 1(b)) in reactions performed in a glass stirred tank reactor (STR). For the F4_MIL-140A(Ce) analogue, the extent of crystallisation, α, was calculated from the second derivative peak area unique to the MOF product. The reaction kinetics determined by non-invasive Raman spectroscopy were in good agreement with those obtained by the synchrotron X-ray diffraction method.[8] Non-invasive Raman spectroscopy also allowed the solution behaviour to be investigated, indicating initial rapid consumption of the nitric acid and ligand source coinciding with a high probability of nucleation, P_N. Thus, non-invasive Raman spectroscopy was demonstrated to be a more accessible technique to study the mechanism of MOF formation. Experimental considerations and limitations of the technique are discussed. An advantage of Raman spectroscopy over X-ray diffraction methods, which can only access information from the solid phase, is that insight is offered into both the solid and solution phases within the reaction medium by a single technique. Therefore, non-invasive Raman spectroscopy is potentially a key enabling tool for the development, optimisation, and scale-up of MOFs.

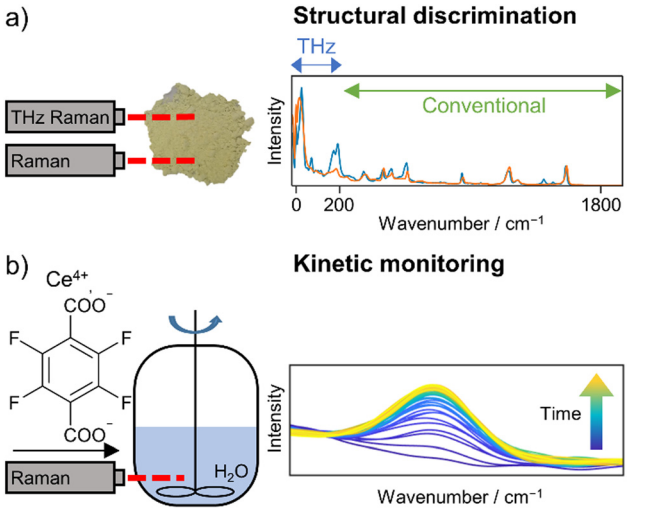

Fig. 1 Use of non-invasive Raman spectroscopy for characterisation of MOFs: (a) rapid discrimination between analogues prepared from the same metal and ligand sources, with particular differences in the THz (or low frequency) region and (b) *in situ* monitoring of MOF formation.

Experimental

General experimental details

Ammonium cerium(IV) nitrate (Sigma-Aldrich, ≥98.5%), copper(II) nitrate hemi(pentahydrate) (Sigma-Aldrich, 98%), *N*,*N*-dimethylformamide (DMF, Sigma Aldrich, ≥99.9%), glacial acetic acid (Sigma-Aldrich, ≥99%), nitric acid (Fisher Scientific, 70%), tetrafluoroterephthalic acid (Fluorochem), and trimesic acid (Sigma-Aldrich, 95%) were purchased from commercial sources and used as received without further purification. Deionised water was obtained from an in-house Milli-Q (Millipore) purification system.

Synthesis and acquisition of off-line THz Raman spectra of MOFs at small-scale

Small-scale experiments were carried out in 7 mL vials; adapted from reported procedures[8] (full details in ESI‡). The vials were heated in a DB5.3 (IKA) heating block with temperature control by a RH Digital (IKA) hotplate. Off-line THz Raman spectra were acquired using a 0.4″ non-contact optic (NCO, Kaiser Optical Systems) attached to a THz-Raman probe head (Ondax) fibre-coupled to an RXN1 Raman spectrometer (Kaiser Optical Systems). The 785 nm CleanLine laser module (Ondax) was operated at 94% power, giving *ca.* 78 mW at source. The spectrometer was operated

using HoloGRAMS (Kaiser Optical Systems) software. A dark current spectrum was obtained prior to spectral acquisition and automatically subtracted from acquired spectra. The THz Raman spectra of the products from the small-scale experiments were measured with the sample within a glass sample vial placed under the non-contact optic. The spectra were measured with an exposure time of 5 s and using 4 accumulations.

Non-invasive *in situ* monitoring of larger scale reactions and off-line analysis of MOFs

For the larger scale reactions a stirred tank reactor (Radleys, 250 mL) was set up and the temperature of the water in the jacket controlled by an Eco RE 420 heater/chiller (Lauda). The temperature was controlled by the internal PT100 resistance temperature detector. The ligand solution was prepared in a Schott bottle (250 mL) and heated to 60 °C in a water bath to dissolve the solid. The target quantities were tetrafluoroterephthalic acid (2.98 g, 12.5 mmol) in either deionised water (175 mL) and nitric acid (25 mL) for F4_MIL-140A(Ce) or deionised water (87 mL), nitric acid (5.7 mL), and acetic acid (107 mL) for F4_UiO-66(Ce). The metal solution of ammonium cerium(IV) nitrate (6.85 g, 12.5 mmol) in deionised water (50 mL) was prepared in a separate Schott bottle (50 mL). The ligand solution was transferred into the STR and stirred at 150 rpm. The Raman probes were positioned around the STR, ensuring all optical components were directed towards the vessel contents. The STR was wrapped in blackout material for protection against accidental exposure to laser irradiation and to block out signals from room lights. Spectral acquisition was started after addition of the ligand solution to the STR, and then the metal solution added to begin the reaction. When the reaction was complete, the solid was isolated by vacuum filtration, washed with deionised water and then washed with acetone.

Non-invasive wide-area illumination Raman spectra were acquired using a PhAT probe (Kaiser Optical Systems) fibre-coupled to an RXN1 Raman spectrometer (Kaiser Optical Systems), with a lens giving a 6 mm spot size, focal distance of 25 cm and focussing tube of *ca.* 20 cm length positioned against the STR. The 785 nm Invictus diode laser (Kaiser Optical Systems) was operated at 350 mW at source. The spectrometer was operated using HoloGRAMS (Kaiser Optical Systems) software. A dark current spectrum was obtained prior to spectral acquisition and automatically subtracted from acquired spectra. Non-invasive *in situ* THz Raman spectra were acquired as using the equipment described for the off-line spectra of the small-scale products, with the optics placed against the glass of the STR. Spectra acquired using the Tornado instrumentation were using a HyperFlux PRO (Tornado Spectral Systems) spectrometer equipped with a 785 nm laser operated at 495 mW and a Hudson S04 (Tornado Spectral Systems) probe head. The Hudson S04 was positioned *ca.* 10 cm from the vessel and the nitric acid signal from test spectra of the ligand solution used to confirm alignment of the probe with the vessel. Acquisition parameters and sampling intervals for the *in situ* spectra are outlined in Table S1 (ESI‡).

Off-line wide-area illumination Raman spectra of isolated MOFs were acquired with the solid material placed underneath the focussing tube of the PhAT probe and using an exposure time of 15 s and 4 accumulations. Off-line THz Raman spectra of the isolated MOFs were acquired with the solid material placed on a laboratory jack underneath the NCO. The focal distance of *ca.* 1 cm was achieved by adjusting the sample to NCO distance to obtain the optimal signal. Each spectrum was acquired with 4 accumulations and an exposure time of 15 s and 30 s for the Experiment 1 and Experiment 3 products, respectively.

Raman data analysis

Analysis of spectra was performed in Matlab (version R2019a, MathWorks) using the GSTools toolbox[51] to import spectral files. Second derivative spectra were calculated using PLS_Toolbox (version 8.6.2, Eigenvector Research) by application of a Savitzky–Golay filter to the full spectra. The second derivative peak intensity of the F4_MIL-140A(Ce) Raman peak at 762 cm^{-1} measured using the PhAT probe in Experiments 1, 2, and 6 was normalised using the minimum and maximum intensity measured for 762 cm^{-1} across the individual experiment. The nitric acid and ligand peak intensities at 1047.6 cm^{-1} and 507.6 cm^{-1}, respectively, measured using the PhAT probe in Experiments 1, 2, and 6 were normalised against the minimum intensity measured at that wavelength for the individual experiment.

Peak areas were calculated by implementation of trapezoidal numerical integration within Matlab. For the F4_MIL-140A(Ce) peak at *ca.* 762 cm^{-1} the second derivative spectra were integrated over the ranges 758.1 to 765.9 cm^{-1} and 758 to 766 cm^{-1} for the PhAT probe and Tornado data, respectively. Similarly, for the F4_UiO-66(Ce) peak at *ca.* 769 cm^{-1} the second derivative spectra were integrated over the ranges 763.8 to 772.2 cm^{-1} and 764 to 773 cm^{-1} for the PhAT probe and Tornado data, respectively. The value for the extent of crystallisation was calculated in a similar procedure to that reported[8] using eqn (1), where α is the extent of crystallisation and A is the second derivative peak area. The terms t, 0, and max denote the time after addition of the metal solution, time zero (coinciding with addition of the metal solution), and the final peak area, respectively.

$$\alpha = \frac{A_t - A_0}{A_{max} - A_0} \quad (1)$$

The times were calculated from timestamps extracted from metadata in the spectral files. Time zero is taken as the spectrum acquired during addition of the metal solution. The data were truncated to include up to 2250 s after addition of the metal solution (approximate end point reported for equivalent conditions).[8]

The second derivative spectra were integrated over the ranges 503.4 to 511.8 cm^{-1} and 503 to 512 cm^{-1} for the PhAT probe and Tornado data, respectively, for the ligand peak at 507 cm^{-1}. Normalisation was performed on the truncated data. The ligand peak area and nitric acid peak intensity were normalised to the minimum value for that experiment/probe

combination, which corresponds to the highest concentration of a negative peak in the second derivative spectra.

Results and discussion

Raman and THz Raman spectroscopy for polymorph discrimination of MOFs

Two Ce MOFs, F4_MIL-140A(Ce) (Fig. 2(a)) and F4_UiO-66(Ce) (Fig. 2(b)), which are analogues prepared from ammonium cerium(IV) nitrate and tetrafluoroterephthalic acid were selected to evaluate the potential use of Raman spectroscopy for polymorph discrimination of MOFs. These MOFs were synthesised at small-scale according to reported procedures[8] and the identity of the products were confirmed by powder X-ray diffraction (PXRD) analysis (Fig. S1, ESI‡). THz Raman spectra were successfully measured for these MOFs using a purpose built instrument.[52,53] The features in the THz region vary substantially between the two different MOFs (Fig. 2(c)). This suggests THz Raman as a promising technique for polymorph discrimination of MOFs, particularly analogues prepared from the same metal sources and ligands with different structures. In the mid frequency Raman region there are also identifying peaks for the two different structures (Fig. 2(d)), for example the CF peak[54] of the tetrafluoroterephthalate ligand at 762 and 768 cm^{-1} for F4_MIL-140A(Ce) and F4_UiO-66(Ce), respectively (Fig. S2, ESI‡). Detailed assignments are outside the scope of this paper, but using the assignments for a UiO-66(Ce) structural analogue as guidance,[55] differences are also observed for the CeO vibrational modes between 200 to 500 cm^{-1} that would be expected between the two analogues (Fig. 2(c)). Compared to PXRD, Raman spectroscopy is a more rapid technique (spectrum acquired in one minute) and sample preparation is not required for analysis.

Non-invasive Raman spectroscopy for *in situ* monitoring of MOF formation and rapid screening of MOF products

As the two Ce MOFs could be successfully characterised by Raman spectroscopy, with identifiable peaks, they were deemed suitable for investigating with larger scale reactions to monitor MOF formation by *in situ* Raman and THz Raman spectroscopy. A 250 mL glass STR permits different monitoring modes. Invasive probes may be positioned within the vessel with the optical lens submerged in the reaction contents. However, restrictions may be posed by the compatibility of the invasive probe with the reaction medium and process conditions. Additionally, the effect of the presence of additional physical components upon crystallisation is unknown. Therefore, the initial experiments commenced with non-invasive monitoring modes. Both Raman and THz Raman spectra were acquired of the same process to allow comparison of their performance for the same reaction. The non-invasive sampling optics differ between the two instruments, with a focussed non-contact optic (100 μm diameter spot) for the THz Raman and wide-area illumination (6 mm diameter spot) available for the Raman instrument. Data acquisition was interleaved to avoid saturation of the THz Raman detector with light from the conventional Raman laser. This is a

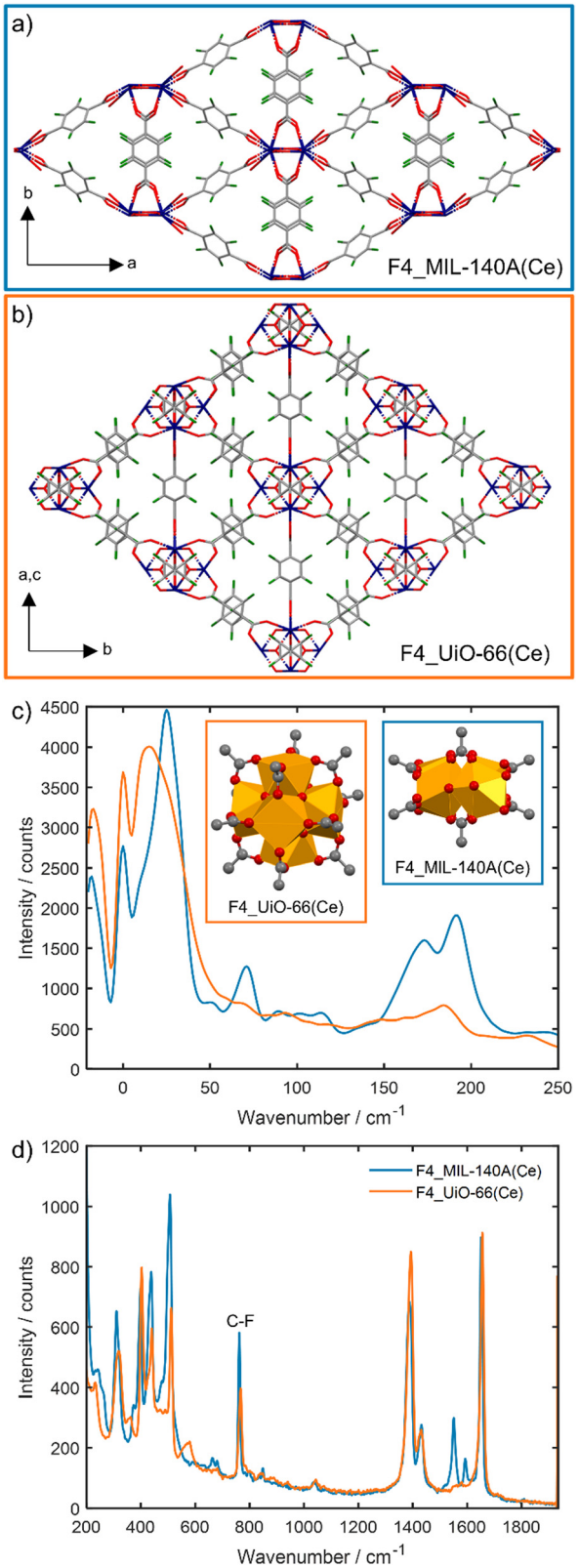

Fig. 2 Structures of (a) F4_MIL-140A(Ce) and (b) F4_UiO-66(Ce).[56] Atom colours are blue, red, grey, and green for cerium, oxygen, carbon, and fluorine, respectively. Raman spectra of products from small-scale reactions: (c) low frequency (or THz) region with the secondary building units of the MOFs (infinite cerium oxide chains with 6-fold connectivity, $Ce_3O_3(CO_2R)_6$, in F4_MIL-140A(Ce) and $Ce_6O_4(OH)_4(CO_2R)_{12}$ in F4_UiO-66(Ce), where R = C_6F_4) and (d) mid frequency Raman region.

Table 1 Summary of large-scale (250 mL) monitoring experiments

Experiment number	System, conditions	Monitoring present
1	F4_MIL-140A(Ce), 60 °C	Non-invasive THz Raman, PhAT probe Raman
2	F4_MIL-140A(Ce), 50 °C	Non-invasive THz Raman, PhAT probe Raman
3	F4_UiO-66(Ce), 60 °C	Non-invasive THz Raman, PhAT probe Raman
4	F4_MIL-140A(Ce), 60 °C	PhAT probe Raman, Tornado Hudson Raman
5	F4_MIL-140A(Ce), 60 °C	PhAT probe Raman, Tornado Hudson Raman
6	F4_MIL-140A(Ce), 60 °C	Invasive Raman, invasive THz Raman, PhAT probe Raman

challenge presented by having multiple light sources present in the same vessel for process analysis.

To assess non-invasive monitoring of the formation of F4_MIL-140A(Ce) in Experiment 1 (Table 1) the PhAT probe and non-contact optic were used for Raman and THz Raman monitoring, respectively (Fig. S3, ESI‡). In the mid frequency Raman spectra, emergence of the F4_MIL-140A(Ce) peak at 762 cm^{-1} is observed over the course of the experiment (Fig. 3); indicating Raman spectroscopy may be used to non-invasively monitor the formation of the MOF. It appears that non-invasive THz Raman monitoring has been unsuccessful for detection of formation of the F4_MIL-140A(Ce) MOF product (Fig. S4, ESI‡).

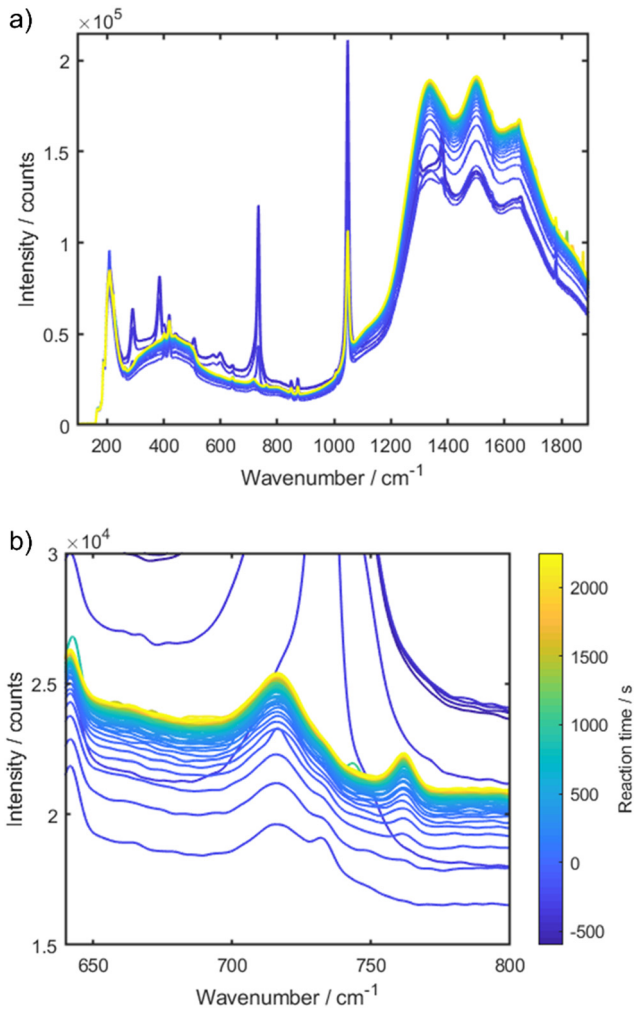

Fig. 3 Raman spectra from non-invasive monitoring of Experiment 1: (a) spectra as acquired and (b) focussing on the region around the F4_MIL-140A(Ce) peak at 762 cm^{-1}. The colour scheme goes from blue to yellow with experiment progress.

A benefit of using Raman spectroscopy is that the nitric acid is also detected, with a characteristic peak[57] at 1048 cm^{-1} observed (Fig. 3(a)). Reference spectra of the components were acquired prior to the experiment (Fig. S5, ESI‡). In the ligand solution there are peaks at 441 and 507 cm^{-1} corresponding to ring bending and OH stretching modes from tetrafluoroterephthalic acid, respectively.[58] For the metal solution there is a peak at 746 cm^{-1} in the reference spectra (Fig. S5, ESI‡). However, this peak is difficult to observe in the spectra from large scale monitoring because of two interferences. Initially, this peak is masked by the polytetrafluoroethylene (PTFE) peak[59] at 733 cm^{-1} originating from the PTFE stirrer (Fig. 3) in the reactor. Then later with the presence of particles from the formation of the MOF product, which changes the sampling depth of the Raman technique owing to scattering, the dominant peak in this region is at 716 cm^{-1} from nitric acid[57] (Fig. 3(b)) which is present at a much higher concentration. Therefore any unreacted metal will likely be at a concentration below the limit of detection. For the conventional Raman monitoring, there is also a large fluorescence glass signal at *ca.* 1500 cm^{-1} observed in the spectra (Fig. 3(a)), which is expected owing to the non-invasive setup (Fig. S3, ESI‡) and wavelength of laser used.[60]

Application of a Savitzky–Golay second derivative filter to the data removes baseline effects and allows for the identification of the peaks of interest in the same position (Fig. S6, ESI‡). Univariate trending of the second derivative F4_MIL-140A(Ce) peak shows that the timescale of the reaction from non-invasive Raman monitoring appears to match the reported time for complete crystallisation of *ca.* 40 min at 60 °C (Fig. 4).[8] Experiment 2 was carried out at a lower temperature (Table 1), with increased spectral acquisition times (Table S1, ESI‡). The Raman monitoring of the MOF peak indicates a slower reaction profile and agreement with the reported time for complete crystallisation in *ca.* 80 min at 50 °C.[8] Non-invasive Raman spectroscopy also enables the behaviour of components in solution to be probed. The depletion of nitric acid is slower for Experiment 2 (Fig. S7, ESI‡), which was carried out at a lower temperature than Experiment 1. Similarly, the depletion of the ligand is also slower for Experiment 2 (Fig. S8, ESI‡). The results of univariate trending of the MOF, ligand, and nitric acid peaks suggest that non-invasive Raman spectroscopy is a suitable technique to obtain mechanistic insight into different components in the reaction medium. Raman spectroscopy is a more broadly applicable technique by potentially providing further

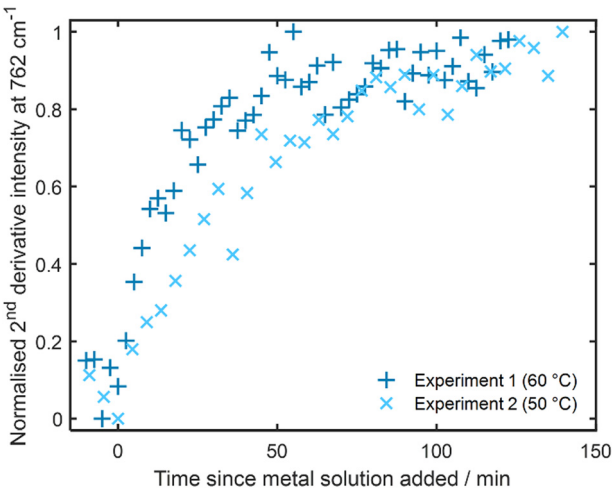

Fig. 4 Normalised intensity of the second derivative F4_MIL-140A(Ce) Raman peak at 762 cm^{-1} with reaction progress for Experiments 1 and 2. NB. 1 corresponds to the highest concentration.

mechanistic insight into all components in the reaction medium, which is not directly offered by X-ray diffraction methods.

Experiment 3 (Table 1) was undertaken with a similar experimental setup to Experiments 1 and 2 (Fig. S3, ESI‡), with non-invasive Raman and THz Raman monitoring of the formation of F4_UiO-66(Ce). The characteristic Raman peaks of F4_UiO-66(Ce), nitric acid, and acetic acid are detected by non-invasive Raman (Fig. S9 and S10, ESI‡). However, the temporal resolution of the spectra (every 150 s) is very slow compared to the expected reaction timescale (300 s).[8] Therefore, to gain insight into the mechanism of the formation of F4_UiO-66(Ce) by non-invasive Raman spectroscopy would require more rapid data acquisition. The characteristic MOF peaks (Fig. 2(c)) were not observed by non-invasive THz Raman monitoring (Fig. S11, ESI‡). Therefore, THz Raman monitoring was not used in the remaining experiments, which removes the need for interleaving the spectrometers for data acquisition, increasing the temporal resolution of the data. To monitor MOF formation *via* non-invasive THz Raman spectroscopy would require further exploration; the lack of success here may be ascribed to the small sampling volume of the non-contact optic used[26] (an accessory allowing for a larger sampling area[61] may be more successful) and lower laser power.

Off-line analysis of the products from Experiments 1 and 3 by THz Raman (Fig. S12, ESI‡) and Raman (Fig. S13, ESI‡) spectroscopy show differences in the spectra between the structural analogues F4_MIL-140A(Ce) and F4_UiO-66(Ce). The identities of the products were confirmed by PXRD analysis to be F4_MIL-140A(Ce) and F4_UiO-66(Ce) for Experiment 1 (Fig. S14, ESI‡) and Experiment 3 (Fig. S15, ESI‡), respectively. This suggests THz Raman and Raman as suitable techniques for rapid solid form screening of the products from MOF reactions (Fig. 1(a)). Detection of the MOF peaks by the PhAT probe in Experiments 1 to 3 also suggest non-invasive Raman spectroscopy could be used to confirm the identity of a synthesis without having to isolate the solid from the reaction medium, which could greatly accelerate screening. This could even be deployed for vessels typically used in screening reactions such as glass vials and pressure tubes.

Kinetic insight determined *via* non-invasive Raman spectroscopy

As non-invasive Raman spectroscopy was demonstrated to be suitable for monitoring MOF formation, Experiments 4 and 5 were performed with additional Raman monitoring from a Tornado HyperFlux PRO instrument with the non-invasive Hudson S04 probe head (4 mm spot size). This instrument benefits from a high throughput virtual slit (HTVS) technology that permits faster measurements.[62] The experimental setup was similar to that used previously, with the Tornado instrument in place of the THz Raman (Fig. S16, ESI‡). The temporal resolution for the PhAT probe monitoring was improved in Experiment 4 (a spectrum every 70 s) and the Tornado permits a much higher temporal resolution (spectra every 10 s). For both instruments, the Raman spectra obtained include a broad glass signal from the STR and is dominated by a nitric acid peak at *ca.* 1047 cm^{-1} (Fig. S17, ESI‡). Using the Hudson, the nitric acid peak intensity is comparable to the glass signal, therefore, the exposure time cannot be increased significantly without saturating the detector. Non-invasive monitoring of the formation of the F4_MIL-140A(Ce) MOF product is improved with the increased temporal resolution (Fig. S18, ESI‡). As the MOF product has a weak intensity, the noisy trend obtained from the Hudson (Fig. S18, ESI‡) is perhaps anticipated, especially with the rapid acquisition time. However, there is the benefit that the behaviour of components in solution, nitric acid (Fig. S19, ESI‡) and ligand (Fig. S20, ESI‡), are captured by non-invasive Raman spectroscopy. As the quantity of acid is a significant factor in the reaction kinetics for the formation of the MOF product,[8] Raman spectroscopy could be proposed as an appropriate technique to probe the role of the acid in the reaction.

Experiment 5 was carried out for monitoring of the F4_MIL-140A(Ce) with optimisation of the exposure time for the Hudson probe. A spectrum every *ca.* 17 s (Table S1, ESI‡) still provides a much higher temporal resolution in comparison to the PhAT probe for non-invasive monitoring. To assess the suitability of Raman spectroscopy for determining reaction kinetics α was calculated from the second derivative peak area in a similar procedure to that reported.[8] The α determined from the PhAT probe data from Experiments 4 and 5 indicate reasonable agreement with the reported kinetics for the F4_MIL-140A(Ce) system at 60 °C with 32 equivalents of nitric acid present (Fig. 5).[8] Some deviations from the reported kinetics are expected owing to experimental differences, such as a significant difference in scale (250 mL herein *vs.* 5 mL reported), stirring mode,[63] and stirring speed (150 rpm here *vs.* 1200 rpm reported), which may have implications on mass transport effects. The α determined from simultaneous Hudson monitoring of the same experiments suggests a different and faster reaction profile (Fig. S21, ESI‡). This may be attributed to the optical properties of the setup, such as differences between

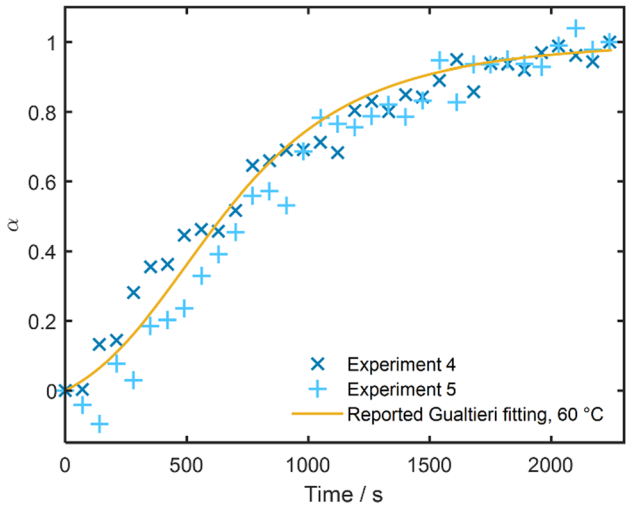

Fig. 5 The extent of crystallisation, α, determined from the second derivative F4_MIL-140A(Ce) peak area at 762 cm^{-1} from non-invasive Raman monitoring *via* the PhAT probe in Experiments 4 and 5 overlaid with the reported Gualtieri fitting as a function of time for the formation of F4_MIL-140A(Ce) at 60 °C in the presence of 32 equivalents of nitric acid.[8]

the probes including sampling volume (4 mm *vs.* 6 mm laser excitation spot for Hudson and PhAT probes, respectively, and different collection optic designs).[64,65] The particle size of material in the solid state and optical configuration of the probe can have a significant contribution to Raman scattering,[66,67] further complicating a direct comparison. The PhAT probe used has been well-characterised previously,[26] however, experimental factors such as working distance have not been fully optimised for the Hudson probe.

Despite the poorer temporal resolution of Raman spectroscopy compared to the synchrotron X-ray diffraction technique, one advantage is that the solution behaviour can also be probed. Overlay of the second derivative nitric acid peak intensity with the reported P_N (Fig. 6)[8] indicates a rapid consumption of nitric acid initially that corresponds to a high P_N. This then drops as P_N decreases, offering an insight into the role of the nitric acid not available from a synchrotron technique that is only sensitive to the solid phase. Whilst the Tornado Hudson is suspected to be extremely sensitive to the scattering properties of particles, the univariate trends of the liquid phase nitric acid are in good agreement between both instruments (Fig. S22, ESI‡). In this instance, the increased temporal resolution from the Tornado Hudson proves advantageous to capturing the kinetic behaviour of the nitric acid.

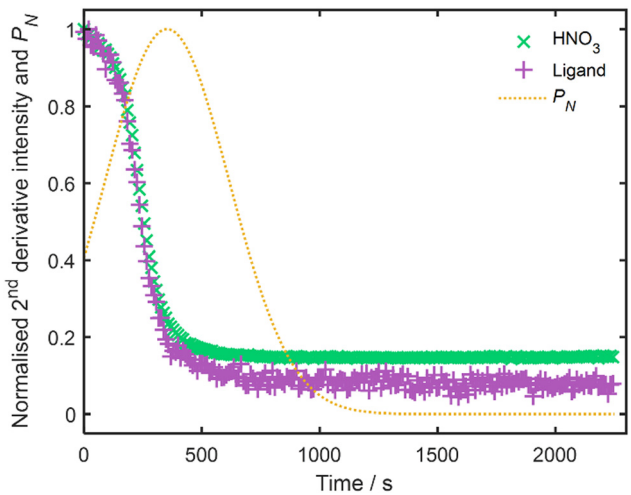

Fig. 6 Change in normalised second derivative intensity of the nitric acid (1047 cm^{-1}) and ligand (507 cm^{-1}) Raman peaks determined by non-invasive Raman monitoring of Experiment 4 using the Tornado Hudson, overlaid against the reported probability of nucleation, P_N, for the formation of F4_MIL-140A(Ce) at 60 °C in the presence of 32 equivalents of nitric acid.[8]

Challenges encountered

During this study, some challenges were encountered that are important to highlight with regards to using Raman spectroscopy, especially for process analysis. As previously discussed, interleaving of the spectrometers was required to avoid saturation of the THz Raman detector. Similarly, with complementary techniques, additional light sources could pose problems for Raman data quality if they also emit at similar wavelengths. For acquisition of all spectra in this study, the experimental setups were covered in blackout material for protection against accidental exposure to laser irradiation and to block out signals from fluorescent room lights.

Sample stability to laser irradiation is also an important consideration and may present a restriction for the deployment of Raman spectroscopy as a technique for monitoring of MOF formation. HKUST-1 was selected as a well-studied MOF,[68] with a reported aqueous room temperature synthetic procedure[69] presenting particularly attractive for Raman monitoring. To acquire reference spectra of the MOF product, HKUST-1 was prepared in batch according to a reported procedure.[70] However, attempted Raman analysis of the product indicated instability to laser irradiation (Fig. S23, ESI‡). Reported Raman studies of HKUST-1 used different excitation wavelengths,[40,71] with a low laser power required to avoid sample decomposition.[72–75] Therefore, HKUST-1 was considered an unsuitable system to pursue further development for *in situ* monitoring with the available Raman instrumentation.

Whilst monitoring of MOF formation was successfully demonstrated for non-invasive monitoring, invasive monitoring modes were also considered for comparison of data quality when the optic is in direct contact with the reagents. Experiment 6 (Table 1) was carried out with three types of Raman monitoring present (Fig. S24, ESI‡): immersion (i) Raman and (ii) THz Raman probes, as well as (iii) the non-invasive Raman PhAT probe. THz Raman monitoring was once again unsuccessful in this instance, with the characteristic low frequency peaks of F4_MIL-140A(Ce) not observed (Fig. S25, ESI‡) even though the optic was immersed in the reaction medium. Reassuringly, the trends for the MOF, nitric acid, and ligand (Fig. S26, S7, and S8, ESI‡ respectively) derived from non-invasive monitoring of Experiment 6 are in agreement with those for Experiment 1, demonstrating reproducibility. Univariate trending of the second derivative MOF peak at 762 cm^{-1}

(Fig. S27, ESI‡) indicates similar trends are obtained with both monitoring modes (Fig. S28, ESI‡). With invasive monitoring, a peak at 748 cm^{-1} is observed upon addition of the metal source (Fig. S27, ESI‡), which is ascribed to the metal source (Fig. S5, ESI‡). This is possible as the PTFE stirrer is not detected in the invasive mode and the concentration of the metal is shown to decrease over the course of the experiment (Fig. S29, ESI‡). Despite the use of a similar immersion Raman probe being reported for monitoring of MOF formation,[14,16,17] the two probes used herein were found to not be entirely compatible with the reaction medium and signs of damage were observed. This highlights the need for caution regarding chemical compatibility of the probe with the reaction medium. In this instance, whilst the invasive probe allows detection of more chemical components, it may also have an unknown effect upon crystallisation such as serving as nucleation sites and is therefore not recommended.

Conclusions

It has been qualitatively demonstrated that non-invasive Raman spectroscopy is a suitable technique for *in situ* monitoring of MOF formation. The sensitivity of the Raman technique to both the solid and liquid phases of the reaction medium has allowed for mechanistic insight into materials present in the solution phase during the formation of the MOFs, which was not obtained from the X-ray diffraction technique.[8] These preliminary investigations demonstrate the feasibility of using non-invasive Raman spectroscopy with scope to further optimise the experimental setup. Quantitative insights would be possible with further development to obtain suitable reference information. Correction of the effects upon spectra from the scattering of light from particles[76,77] could also lead to improved data interpretation. It may be possible to acquire higher time resolution data, by reducing the acquisition time for each spectrum, and still obtain spectra of sufficient quality for mechanistic insights. The sensitivity of the Raman techniques to structural analogues also provides scope to utilise this in mixed phase systems or for deployment as rapid screening tools. These advances demonstrate that significant insights may be elucidated *via* non-invasive Raman spectroscopy, and show that it can be a powerful analytical technique for the commercialisation of MOFs.

Author contributions

Conceptualisation: M. W. S. C., A. J. P.; data curation: M. W. S. C., A. J. P., D. J. A.; formal analysis: M. W. S. C., A. J. P., D. J. A.; funding acquisition: M. W. S. C., A. J. P., A. J. F., A. N.; investigation: M. W. S. C., A. J. P.; methodology: M. W. S. C., A. J. P.; project administration: M. W. S. C., A. J. P.; resources: A. J. F., A. N.; supervision: A. J. F.; A. N.; visualisation: M. W. S. C.; A. J. P., D. J. A; writing – original draft: M. W. S. C.; writing – review and editing: M. W. S. C., A. J. P., D. J. A., A. J. F., A. N.

Conflicts of interest

There are no conflicts to declare.

Acknowledgements

M. W. S. C. and A. J. P. are grateful to ScotCHEM for the non-independent ECR funding that was used for purchase of reagents in this work. M. W. S. C., A. J. P. and D. J. A. are grateful to the EPSRC (grant ref: EP/P006965/1), the Centre for Process Analytics and Control Technology (CPACT) and the EPSRC (grant ref: EP/T034114/1), respectively, for funding. The authors acknowledge that some of the experimental work presented was carried out in the CMAC National Facility, housed within the University of Strathclyde's Technology and Innovation Centre, and funded with a UK Research Partnership Institute Fund (UKRPIF) capital award, Scottish Funding Council (SFC) ref. H13054, from the Higher Education Funding Council for England (HEFCE). The authors would like to thank Clairet Scientific Ltd. for the loan of the Tornado instrument. We are grateful to Alex Clunie for CHN analysis. Charlie O'Hara is thanked for helpful discussions about the paper and their valuable suggestions.

References

1 J. H. ter Horst, C. Schmidt and J. Ulrich, *Handbook of Crystal Growth: Bulk Crystal Growth*, Elsevier Inc., 2nd edn, 2015, vol. 2, pp. 1317–1349.
2 M. J. Van Vleet, T. Weng, X. Li and J. R. Schmidt, *Chem. Rev.*, 2018, **118**, 3681–3721.
3 C.-C. Hou, Q. Xu, C.-C. Hou and Q. Xu, *Adv. Energy Mater.*, 2019, **9**, 1801307.
4 V. Bon, *Curr. Opin. Green Sustain. Chem.*, 2017, **4**, 44–49.
5 Z. Zhou, M. Vázquez-González and I. Willner, *Chem. Soc. Rev.*, 2021, **50**, 4541–4563.
6 Y. Wen, P. Zhang, V. K. Sharma, X. Ma and H. C. Zhou, *Cell Rep. Phys. Sci.*, 2021, **2**, 100348.
7 C. Duan, Y. Yu, J. Xiao, Y. Li, P. Yang, F. Hu and H. Xi, *Green Energy Environ.*, 2021, **6**, 33–49.
8 S. J. I. Shearan, J. Jacobsen, F. Costantino, R. D'Amato, D. Novikov, N. Stock, E. Andreoli and M. Taddei, *Chem. – Eur. J.*, 2021, **27**, 6579–6592.
9 B. He, L. K. Macreadie, J. Gardiner, S. G. Telfer and M. R. Hill, *ACS Appl. Mater. Interfaces*, 2021, **13**, 54284–54293.
10 F. C. N. Firth, M. W. Gaultois, Y. Wu, J. M. Stratford, D. S. Keeble, C. P. Grey and M. J. Cliffe, *J. Am. Chem. Soc.*, 2021, **143**, 19668–19683.
11 C. L. Jones, C. E. Hughes, H. H.-M. Yeung, A. Paul, K. D. M. Harris and T. L. Easun, *Chem. Sci.*, 2021, **12**, 1486–1494.
12 J. Ren, N. M. Musyoka, H. W. Langmi, B. C. North, M. Mathe, W. Pang, M. Wang and J. Walker, *Appl. Surf. Sci.*, 2017, **404**, 263–267.
13 J. Zhao, B. Kalanyan, H. F. Barton, B. A. Sperling and G. N. Parsons, *Chem. Mater.*, 2017, **29**, 8804–8810.
14 H. Embrechts, M. Kriesten, K. Hoffmann, W. Peukert, M. Hartmann and M. Distaso, *J. Phys. Chem. C*, 2018, **122**, 12267–12278.

15 H. Embrechts, M. Kriesten, M. Ermer, W. Peukert, M. Hartmann and M. Distaso, *RSC Adv.*, 2020, **10**, 7336–7348.
16 H. Embrechts, M. Kriesten, M. Ermer, W. Peukert, M. Hartmann and M. Distaso, *Cryst. Growth Des.*, 2020, **20**, 3641–3649.
17 H. Embrechts, M. Hartmann, W. Peukert and M. Distaso, *Chem. Eng. Technol.*, 2020, **43**, 879–886.
18 J. McGinty, M. W. S. Chong, A. Manson, C. J. Brown, A. Nordon and J. Sefcik, *Crystals*, 2020, **10**, 925.
19 A. Borissova, S. Khan, T. Mahmud, K. J. Roberts, J. Andrews, P. Dallin, Z.-P. Chen and J. Morris, *Cryst. Growth Des.*, 2009, **9**, 692–706.
20 Jochen Schöll, Davide Bonalumi, L. Vicum, M. Mazzotti and M. Müller, *Cryst. Growth Des.*, 2006, **6**, 881–891.
21 M. Vendel and Å. C. Rasmuson, *AIChE J.*, 1997, **43**, 1300–1308.
22 A. Nordon, A. Mills, R. T. Burn, F. M. Cusick and D. Littlejohn, *Anal. Chim. Acta*, 2005, **548**, 148–158.
23 K. A. Esmonde-White, M. Cuellar, C. Uerpmann, B. Lenain and I. R. Lewis, *Anal. Bioanal. Chem.*, 2017, **409**, 637–649.
24 L. L. Simon, H. Pataki, G. Marosi, F. Meemken, K. Hungerbühler, A. Baiker, S. Tummala, B. Glennon, M. Kuentz, G. Steele, H. J. M. Kramer, J. W. Rydzak, Z. Chen, J. Morris, F. Kjell, R. Singh, R. Gani, K. V. Gernaey, M. Louhi-Kultanen, J. O'Reilly, N. Sandler, O. Antikainen, J. Yliruusi, P. Frohberg, J. Ulrich, R. D. Braatz, T. Leyssens, M. von Stosch, R. Oliveira, R. B. H. Tan, H. Wu, M. Khan, D. O'Grady, A. Pandey, R. Westra, E. Delle-Case, D. Pape, D. Angelosante, Y. Maret, O. Steiger, M. Lenner, K. Abbou-Oucherif, Z. K. Nagy, J. D. Litster, V. K. Kamaraju and M.-S. Chiu, *Org. Process Res. Dev.*, 2015, **19**, 3–62.
25 R. A. Halliwell, R. M. Bhardwaj, C. J. Brown, N. E. B. Briggs, J. Dunn, J. Robertson, A. Nordon and A. J. Florence, *J. Pharm. Sci.*, 2017, **106**, 1874–1880.
26 P. Allan, L. J. Bellamy, A. Nordon, D. Littlejohn, J. Andrews and P. Dallin, *J. Pharm. Biomed. Anal.*, 2013, **76**, 28–35.
27 P. Hamilton, D. Littlejohn, A. Nordon, J. Sefcik, P. Slavin, J. Andrews and P. Dallin, *Chem. Eng. Sci.*, 2013, **101**, 878–885.
28 P. Hamilton, D. Littlejohn, A. Nordon, J. Sefcik, P. Slavin, P. Dallin and J. Andrews, *Analyst*, 2011, **136**, 2168–2174.
29 G. Févotte, *Chem. Eng. Res. Des.*, 2007, **85**, 906–920.
30 C. Xiouras, G. Belletti, R. Venkatramanan, A. Nordon, H. Meekes, E. Vlieg, G. D. Stefanidis and J. H. Ter Horst, *Cryst. Growth Des.*, 2019, **19**, 5858–5868.
31 A. J. Parrott, P. Dallin, J. Andrews, P. M. Richardson, O. Semenova, M. E. Halse, S. B. Duckett and A. Nordon, *Appl. Spectrosc.*, 2019, **73**, 88–97.
32 S. Mozharov, A. Nordon, D. Littlejohn, C. Wiles, P. Watts, P. Dallin and J. M. Girkin, *J. Am. Chem. Soc.*, 2011, **133**, 3601–3608.
33 D. R. Du Bois, K. R. Wright, M. K. Bellas, N. Wiesner and A. J. Matzger, *Inorg. Chem.*, 2022, **61**, 4550–4554.
34 C. Leroy, T.-X. Métro, I. Hung, Z. Gan, C. Gervais and D. Laurencin, *Chem. Mater.*, 2022, **34**, 2292–2312.
35 N. Townshend, A. Nordon, D. Littlejohn, M. Myrick, J. Andrews and P. Dallin, *Anal. Chem.*, 2012, **84**, 4671–4676.
36 K. Bērziņš, S. J. Fraser-Miller and K. C. Gordon, *Int. J. Pharm.*, 2021, **592**, 120034.
37 M. R. Ryder, B. Van de Voorde, B. Civalleri, T. D. Bennett, S. Mukhopadhyay, G. Cinque, F. Fernandez-Alonso, D. De Vos, S. Rudić and J.-C. Tan, *Phys. Rev. Lett.*, 2017, **118**, 255502.
38 A. E. J. Hoffman, L. Vanduyfhuys, I. Nevjestić, J. Wieme, S. M. J. Rogge, H. Depauw, P. Van Der Voort, H. Vrielinck and V. Van Speybroeck, *J. Phys. Chem. C*, 2018, **122**, 2734–2746.
39 L. Hanna and J. V. Lockard, *J. Phys.: Condens. Matter*, 2019, **31**, 483001.
40 M. R. Ryder, B. Civalleri, G. Cinque and J.-C. Tan, *CrystEngComm*, 2016, **18**, 4303–4312.
41 M. Premila, A. Bharathi, R. Rajaraman, S. Hussain, P. D. Babu, C. S. Sundar and G. Amarendra, *J. Raman Spectrosc.*, 2018, **49**, 549–558.
42 S. Kusaka, Y. Nakajima, A. Hori, A. Yonezu, K. Kikushima, W. Kosaka, Y. Ma and R. Matsuda, *Faraday Discuss.*, 2021, **225**, 70–83.
43 Q. Li, A. J. Zaczek, T. M. Korter, J. A. Zeitler and M. T. Ruggiero, *Chem. Commun.*, 2018, **54**, 5776–5779.
44 A. Krylov, A. Vtyurin, P. Petkov, I. Senkovska, M. Maliuta, V. Bon, T. Heine, S. Kaskel and E. Slyusareva, *Phys. Chem. Chem. Phys.*, 2017, **19**, 32099–32104.
45 A. Krylov, I. Senkovska, S. Ehrling, M. Maliuta, S. Krylova, E. Slyusareva, A. Vtyurin and S. Kaskel, *Chem. Commun.*, 2020, **56**, 8269–8272.
46 L. Abylgazina, I. Senkovska, S. Ehrling, V. Bon, P. St. Petkov, J. D. Evans, S. Krylova, A. Krylov and S. Kaskel, *CrystEngComm*, 2021, **23**, 538–549.
47 W. Lu, E. Zhang, J. Qian, C. Weeraratna, M. N. Jackson, C. Zhu, J. R. Long and M. Ahmed, *Phys. Chem. Chem. Phys.*, 2022, **24**, 26102–26110.
48 J. Jacobsen, A. Ienco, R. D'Amato, F. Costantino and N. Stock, *Dalton Trans.*, 2020, **49**, 16551–16586.
49 Z. Hu, Y. Wang and D. Zhao, *Chem. Soc. Rev.*, 2021, **50**, 4629–4683.
50 K. I. Hadjiivanov, D. A. Panayotov, M. Y. Mihaylov, E. Z. Ivanova, K. K. Chakarova, S. M. Andonova and N. L. Drenchev, *Chem. Rev.*, 2020, **121**, 1286–1424.
51 K. De Gussem, J. De Gelder, P. Vandenabeele and L. Moens, *Chemom. Intell. Lab. Syst.*, 2009, **95**, 49–52.
52 C. Moser and F. Havermeyer, *AIP Conf. Proc.*, 2010, **1267**, 794–795.
53 C. Moser and F. Havermeyer, *US Pat.*, 7986407 B2, 2011.
54 F. Menaa, B. Menaa and O. Sharts, *Faraday Discuss.*, 2011, **149**, 269–278.
55 A. Airi, C. Atzori, F. Bonino, A. Damin, S. Øien-ØDegaard, E. Aunan and S. Bordiga, *Dalton Trans.*, 2020, **49**, 12–16.
56 R. D'Amato, A. Donnadio, M. Carta, C. Sangregorio, D. Tiana, R. Vivani, M. Taddei and F. Costantino, *ACS Sustainable Chem. Eng.*, 2019, **7**, 394–402.
57 T. Langner, A. Rietig and J. Acker, *J. Raman Spectrosc.*, 2020, **51**, 366–372.

58 F. Li, Z. Zheng, S. Xia and L. Yu, *J. Mol. Struct.*, 2020, **1219**, 128480.
59 J. L. Koenig, F. J. Boerio, I. J. L. Koenig and F. J. Boehio, *J. Chem. Phys.*, 1969, **50**, 2823–2829.
60 D. Tuschel, *Spectroscopy*, 2016, **31**, 14–23.
61 THz-Raman® FloodLightTM Sampling Accessory, **https://content.coherent.com/legacy-assets/pdf/FloodLight_Accessory_Datasheet_August_2018.pdf**, (accessed May 2022).
62 J. T. Meade, A. R. Hajian, B. B. Behr and A. T. Cenko, *US Pat.*, 8958065 B2, 2015.
63 A. A. Zlota, in *Polymorphism in the Pharmaceutical Industry*, ed. R. Hilfiker and M. von Raumer, John Wiley & Sons, Ltd, 2nd edn, 2018, pp. 305–328.
64 H. Owen, D. J. Strachan, J. B. Slater and J. M. Tedesco, *US Pat.*, 7148963 B2, 2006.
65 B. B. Behr and S. Driver, *WO Pat.*, 2021/163807 A1, 2021.
66 H. Wang, C. K. Mann and T. J. Vickers, *Appl. Spectrosc.*, 2016, **56**, 1538–1544.
67 M. V. Pellow-Jarman, P. J. Hendra and R. J. Lehnert, *Vib. Spectrosc.*, 1996, **12**, 257–261.
68 S. S.-Y. Chui, S. M.-F. Lo, J. P. H. Charmant, A. G. Orpen and I. D. Williams, *Science*, 1999, **283**, 1148–1150.
69 J. Huo, M. Brightwell, S. El Hankari, A. Garai and D. Bradshaw, *J. Mater. Chem. A*, 2013, **1**, 15220–15223.
70 C. McKinstry, E. J. Cussen, A. J. Fletcher, S. V. Patwardhan and J. Sefcik, *Chem. Eng. J.*, 2017, **326**, 570–577.
71 J. Bae, S. H. Park, D. Moon and N. C. Jeong, *Commun. Chem.*, 2022, **5**, 51.
72 F. S. Gentile, M. Pannico, M. Causà, G. Mensitieri, G. Di Palma, G. Scherillo and P. Musto, *J. Mater. Chem. A*, 2020, **8**, 10796–10812.
73 M. Todaro, A. Alessi, L. Sciortino, S. Agnello, M. Cannas, F. M. Gelardi and G. Buscarino, *J. Spectrosc.*, 2016, **2016**, 8074297.
74 N. R. Dhumal, M. P. Singh, J. A. Anderson, J. Kiefer and H. J. Kim, *J. Phys. Chem. C*, 2016, **120**, 3295–3304.
75 C. Prestipino, L. Regli, J. G. Vitillo, F. Bonino, A. Damin, C. Lamberti, A. Zecchina, P. L. Solari, K. O. Kongshaug and S. Bordiga, *Chem. Mater.*, 2006, **18**, 1337–1346.
76 Z.-P. Chen, L.-M. Li, J.-W. Jin, A. Nordon, D. Littlejohn, J. Yang, J. Zhang and R.-Q. Yu, *Anal. Chem.*, 2012, **84**, 4088–4094.
77 J.-W. Jin, Z.-P. Chen, L.-M. Li, R. Steponavicius, S. N. Thennadil, J. Yang and R.-Q. Yu, *Anal. Chem.*, 2012, **84**, 320–326.